Practical procedure for the precise measurement of geometrical tendon positions in concrete with ultrasonic echo

Stefan Maack[1*], *Stefan* Küttenbaum[1], and *Ernst* Niederleithinger[1]

[1]Bundesanstalt für Materialforschung und -prüfung (BAM), D-12557 Berlin, Germany

Abstract. Existing concrete structures were usually designed for lifetimes of several decades. The current and urgently required efforts to increase sustainability and protect the environment will likely result in extended service lives up to 100 years. To achieve such objectives, it is required to assess structures over their entire lifecycles. Non-destructive testing (NDT) methods can reliably support the assessment of existing structures during the construction, operational, and decommissioning phases. One of the most important and safety-relevant components of a prestressed concrete structure are the tendons. NDT methods such as the ultrasonic echo method are suitable for both the detection and the localization of the tendons, i.e., the measurement of their geometrical position inside the component. The uniqueness of structures, concrete heterogeneity, and varying amounts of secondary components such as the reinforcement represent obstacles in the application of these methods in practice. The aim of this contribution is to demonstrate a practicable procedure, that can be used in the field to determine the parameters required for the measuring data analysis without extensive knowledge about the investigated components. For this purpose, a polyamide reference specimen is used to show which steps are required to obtain reliable imaging information on the position of tendons from the measurement data. The procedure is then demonstrated on a concrete test specimen that covers various relevant and practice-oriented test scenarios, such as varying tendon depths and component thicknesses.

1 Introduction

The general requirements imposed on modern concrete structures are continuously increasing. Engineers and architects are nowadays required to consider not only the expected safety and durability of a structure, but also other aspects such as sustainability, resilience, climate protection and the socio-economic environment. Two of the ways in which these objectives can be reached is the use of digital models of structures and computer-aided advanced numerical analysis methods. Based on digital models (e.g., Building Information Modeling, BIM), the design and assessment, the construction and maintenance works, the management during the operational phase and the decommissioning can be controlled and performed efficiently and consecutively throughout the entire life cycle. The computational verification of the performance and serviceability of a structure can be assessed using partially established advanced computation methods such as non-linear finite element analyses or, in some cases, probabilistic calculations. In order to assess a structure as realistically (in the sense of: precisely), the various input parameters, such as the "true" position of tendons, must be known. Determining these input parameters is a major challenge in civil engineering and vitally important, since differences between the original planning and the actual as-built situation are frequently observed in practice. These may be caused by changes that have been found to be necessary during the construction phase or may also result from an initially uncertain range in the quality of the supplied materials (e.g., concrete strength). Although this and other issues are covered in semi-probabilistic design and assessment, it follows from the safety elements like standardized partial safety factors, that the structures are commonly planned conservatively. Thus, many structures feature computational "reserves". If the built environmental conditions, such as traffic loads or climate, change during the life cycle of a structure it may be necessary to mobilize these reserves for a successful (re-) assessment. In this case, the condition of the structure should be sufficiently known.

Over the last decades, non-destructive testing methods for civil engineering (NDT CE) have been established as an important tool for determining crucial characteristics of an existing structure. An initial overview of the practical application of various test methods for the examination of concrete structures is given, for example, in [1-5]. Most of the non-destructive testing methods described in these references have already reached a generally recognized *state of the art*. A basic prerequisite for achieving this state of the art is that the performance of the test methods and the quality of the results can be demonstrated. Proof of the capability of a test procedure can be provided, e.g., using the POD (*Probability Of Detection*) method. This approach can be applied for a given test procedure to state the probability with which the testing task can be solved

* Corresponding author: stefan.maack@bam.de

reliably. Examples can be found in [6-9]. In addition to the performance, the evaluation of the quality of the results also plays an important role, for example in order to be able to compare the results of different test methods. One approach is the application of the GUM (Guide to the Expression of Uncertainty in Measurement) framework [10,11]. Once the performance of the method and quality of the results have been analyzed, the testing methods can be used as sound source of information in the assessment of structures. The methodology as well as practical examples for the use of measured values in reliability assessment can be found in [12-16]. The application of measurement results in the assessments of existing structures will be taken into account in future recommendations for national standardization [17,18].

This contribution demonstrates how measurement data of non-destructive testing can be evaluated in order to map the internal structure of structural concrete components. The presented case study is the geometrical reconstruction of the position of tendons inside a test specimen built at the Federal Institute for Materials Research and Testing (BAM) in Berlin. Tendons are structural components that have a considerable potential to endanger structural safety e.g., in the case of damage and degradation. In principle, different NDT methods (e.g., Ground Penetrating Radar (GPR), Ultrasonic echo method) can be used to solve the inspection task "tendon location". If there is a high density of near-surface reinforcement and/or the mounting depth of the tendons is comparatively high, the ultrasonic echo method is preferred despite the more time-consuming measurements. The evaluation method presented here is demonstrated using ultrasonic echo measurements. This method does not require any prior knowledge about the acoustic material properties of the investigated structure. This is a great advantage considering the strong material variations in concrete structures. In addition, it is shown where the limits of the method are and what accuracy can be expected in locating the tendons by on-site testing.

2 Ultrasonic echo method

The principle of the ultrasonic echo method is shown in Fig. 1. A probe is placed on the surface and sends a short pulse into the component (transmitter (T)). The pulse propagates through the measuring object at a material-dependent velocity *(c)*. If it encounters an interface at which the acoustic material properties change, parts of the pulse are reflected and other parts pass through the interface in transmission. As shown in Fig. 1, typical interfaces in concrete components are the tension strands of tendons (case (a)), the back wall of a component (case (b)) or the transition from screed to concrete (case (c)). The part of the pulse reflected at the interface then returns the measuring surface and is sampled there by the receiver (R) of the test probe. With increasing travel path through the component, the pulse is continuously weakened. The reasons for this are scattering at the aggregates, absorption and divergence of the pulse.

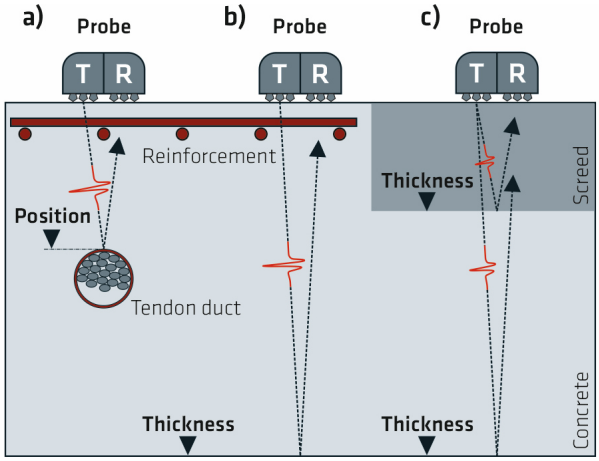

Fig. 1. Different testing scenarios of the ultrasound echo method (dotted line – path of the pulse, red solid line – impulse shape after a certain propagation time) [19]

State of the art is that the test probes for concrete testing operate without coupling agents. Due to the heterogeneous material properties of concrete, transverse waves (SH waves: shear horizontal) are usually used. This kind of wave is significantly less sensitive to the sound-attenuating effects of scattering by the aggregates.

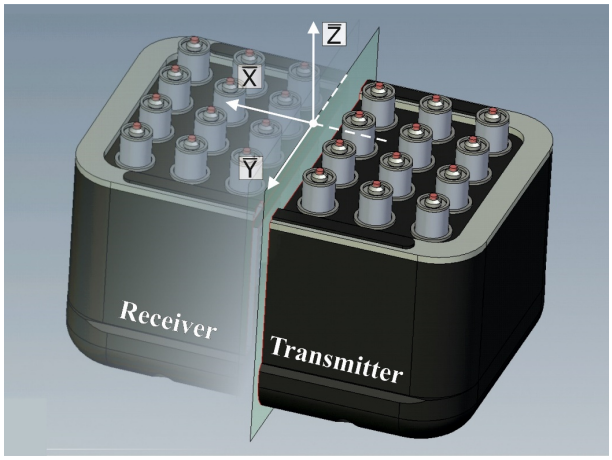

Fig. 2. Low frequency ultrasonic array made of 24 single probes (12 receivers, 12 transmitters) [20]

Fig. 2 shows a drawing of the applied probe looking at the contact surface to the component. The array consists of 24 single probes, with 12 probes transmitting and 12 probes receiving simultaneously. The geometrical spacing from the centers of the receivers and transmitters is approx. $a = 6\ cm$. The single probes have a distance of $a = 2\ cm$ from each other. The probes operate in a frequency range of $f = 25\text{-}75\ kHz$ with a mean frequency of $f_m = 55\ kHz$ and a bandwidth of $B = 25\ kHz$. The excited transverse wave is polarized in the $\bar{Y}$ direction.

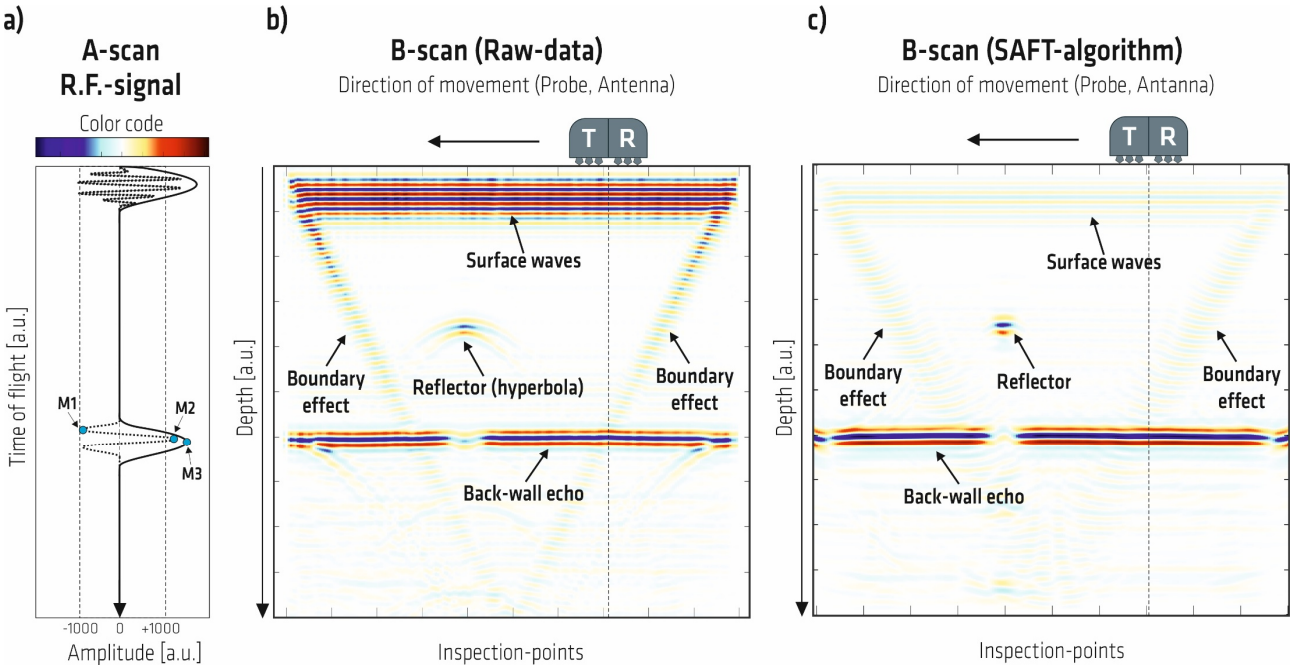

Fig. 3. Types of representation for imaging ultrasonic signals from single pulse (A-scan, (a)) to raw data (B-scan, (b)) and reconstructed data (B-scan, (c)). (Ultrasonic data recorded on test specimen "Pk218" Fig. 6, source of data [20]).

As described above, the probe sends a short acoustic pulse into the component and then receives it again after a certain travel time. The measurement is therefore a time-of-flight measurement in which the measured quantity is the time *(t)* it takes the pulse to travel through the object. A single measurement can be represented graphically in a time-of-flight diagram (A-scan). Such an A-scan can be seen on the left of Fig. 3 (a). Typical signal representations are an oscillating alternating signal (dashed line) and a processed waveform of the same signal (magnitude, solid line). If several measuring points are recorded along a defined measuring line, an imaging representation can be made from this by color-coding the respective amplitudes of the A-scans. This type of imaging is called a B-scan and can be seen in Fig. 3 (b). In a B-scan, changes in the signal image caused by reflecting objects (e. g. tendon) can be detected very easily and spatially assigned along the measurement line. As can be seen in the B-scan of the raw data, a wide variety of signal components are received due to the spatial propagation of ultrasonic waves in the component. These include, for example, surface waves, boundary effects as well as diffraction hyperbolas on point-shaped objects (e.g. tendons). With complicated geometries of the component and a large number of tendons, this can quickly lead to superimposition effects that are very difficult to interpret. Therefore, the raw data is usually post-processed using a reconstruction algorithm (e. g. SAFT - Synthetic Aperture Focusing Technique). By using this post-processing, interfering effects (e. g. surface waves) can be suppressed and the signal images of point-shaped reflectors can be focused on their geometrical origin. The result of such a reconstruction can be seen in Fig. 3 (c). To derive a geometrically accurate representation of the inner structure of components, various input parameters are required to perform the reconstruction calculations. The input parameters include the dimensions of the aperture (probe, Fig. 2), the knowledge of the characteristics of the radiated sound field as well as the velocity *(c)* of the excited ultrasonic wave. In particular, the analysis of the sound velocity *(c)* represents a challenge, as it is subject to large variations depending on the respective concrete mixture. Since it is not always possible to calibrate the sound velocity directly on the component, the following section shows how this can be done using only the recorded ultrasonic signals.

To be able to calculate the sound velocity, the transit time *(t)* and the travel path *(d)* of the pulse in the material are required. The transit time (t_G) measured by the measuring instrument is made up of two components: on the one hand, the transit time *(t)* required by the pulse to travel from the transmitter to the receiver. On the other hand, there is a part which consists of time components which are technically needed within the measuring equipment to generate the pulse. This time is referred to as offset, yields time zero (t_0) and must be subtracted from the measured transit time (t_G) to observe unbiased values.

An additional challenge is to detect the actual first arrival of the acoustic pulse on a real signal. This is often not possible due to structural noise. For this reason, reference points must be defined in the ultrasonic signal. Typical reference points (M1, M2, M3) are shown in Fig. 3 (a) and Fig. 4. This means, in turn, that the calculated velocity is related to the selected reference point ($\bar{c}^{M1,M2,M3}$), which deviates from the true value (material constant). Another phenomenon needed for the sound velocity calculation are the so-called multiple echoes. These occur when the pulse

* Corresponding author: stefan.maack@bam.de

is reflected several times between an interface (e.g., the back wall of the component) and the opposite surface (e.g., the measuring area). With an increasing number of reflections, the sound pulse becomes continuously weaker (Fig. 4, (a)) and also changes its signal shape (Fig. 4, (b)).

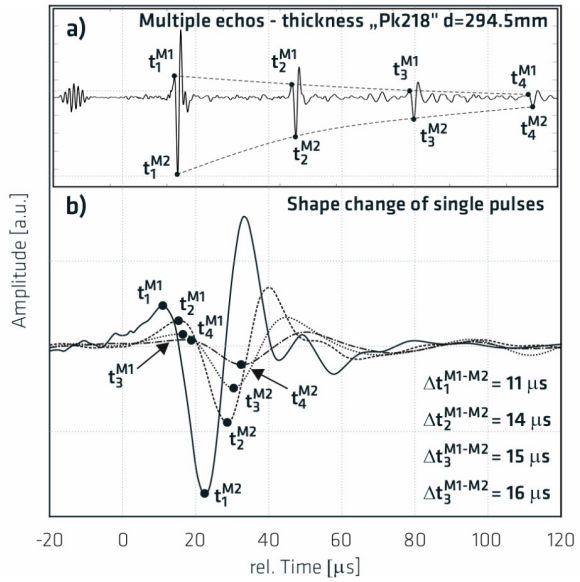

Fig. 4. Multiple signals (echoes) (a) and change of waveform (b) of an averaged ultrasonic pulse (transverse wave $f_m = 55\ kHz$) on the BAM reference specimen "Pk218" (source of data [20]).

The travel path *(d)* of the pulse is calculated from the component thickness, taking into account the geometrical distance of $a_{TR} = 6\ cm$ between transmitter and receiver (Fig. 2). This is a simplified assumption which, e.g., does not account for distortions in the reception of the pulse due to the influence of surface waves.

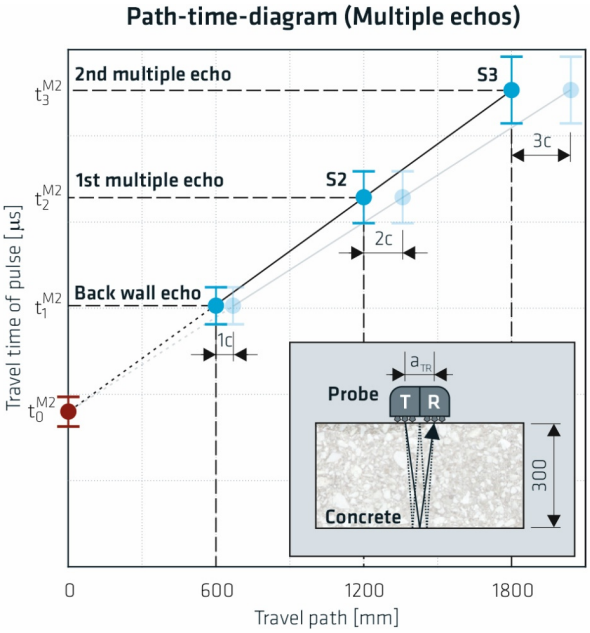

Fig. 5. Relationship between transit time and increase in travel path in the case of multiple reflection of the sound impulse at the back wall of the structural component [19]

The principle of calculating the related sound velocity $(\overline{c})$ and the time zero (t_0) is shown in Fig. 5. The effect of multiple echoes and the associated doubling of the travel path of the pulse through the component is used here. It is assumed that the surface and the back wall of the component are parallel. To minimize influences from the coupling of the probe as well as scattering caused by the aggregate, a series of measuring points is recorded. Subsequently, the respective measured values of the backwall echo and the multiple echoes are assigned to the respective travel paths. The consideration of several measurement points yields a number of observed values, from which the variance (i.e., the squared standard deviation of the mean in this specific case) can be estimated. Applying linear regression (simplified assumption) in combination with a Monte Carlo Simulation according to [11], the time zero (t_0) and the sound velocity $(\overline{c})$ with the assigned variances can be calculated afterwards. The basic procedure is shown below in the first step using a reference specimen made of polyamide. For this specimen, the measurement data are freely available (open access) [20] and the proposed procedure can be reproduced. In the second step, the evaluation and comparison are then carried out on a concrete specimen.

3 Reference specimen

The schematic procedure for determining the sound velocity $(\overline{c})$ and the time zero (t_0) solely on the basis of the measured data is demonstrated using the BAM reference specimen with the internal designation "Pk218". The reference specimen consists of the material polyamide. This has the advantage that there are no sound attenuation effects due to scattering, such as on the aggregate in the concrete. The specimen has a length of $l = 1000\ mm$, a width of $b = 600\ mm$ and a thickness of $d = 294.5\ mm$. In addition, a hole has been drilled horizontally through the specimen with a diameter $D = 50\ mm$, which corresponds in its dimension to a tendon duct (Fig. 6).

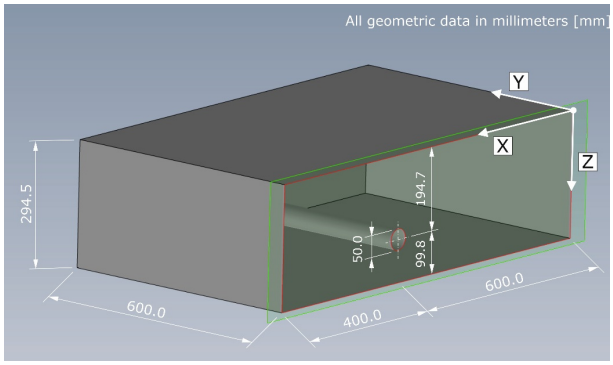

Fig. 6. 3D technical drawing showing the geometrical dimensions of the BAM reference specimen ”Pk218“ made of polyamide with borehole [20].

The specimen was scanned with an automated measuring system developed at BAM and using the probe shown in Fig. 2. The measurement data obtained are available as an

open access file [15]. The aim is to show how the selection of the parameters as well as the applied procedure affect the results of the geometrical reconstruction. 12 possible variants are investigated. These include 6 variants each in which the different possible reference points in the signal image (Fig. 3 (a): M1, M2, M3), as well as the number of supporting points (Fig. 5: S2 - backwall echo + 1st multiple echo; S3 - backwall echo + 1st multiple echo + 2nd multiple echo) are varied. 6 further variants result from the consideration of the additional travel path (distance error) caused by the geometrical spacing (a_{TR}) between transmitter and receiver at the probe.

Table 1. *Extract results of the calculation of the sound velocity ($\bar{c}$) and time zero (t_0)*

	Reference point	Velocity ($\bar{c}$) [m/s]	Time zero (t_0) [µs]
Variation S2	M1	1136.58±0.1464	16.00±0.0858
	M2	1133.32±0.1624	27.07±0.0932
	M3	1135.05±0.1925	31.26±0.1055

Table 1 shows extracts of the results of the calculation of the sound velocities and the time zero for the different reference points at 2 supporting points (S2 - backwall echo + 1st multiple echo). The velocity and the time zero vary depending on the selected reference point. With the input parameters calculated in this way, the reconstruction calculations were then performed using the SAFT algorithm (software: InterSAFT, University of Kassel (Dr. Klaus Mayer)) [21]. Fig. 7 shows an example of the result of the reconstruction in a B-scan for reference point M3. The deviations from the actual geometry are derived as an average value from all B-scans.

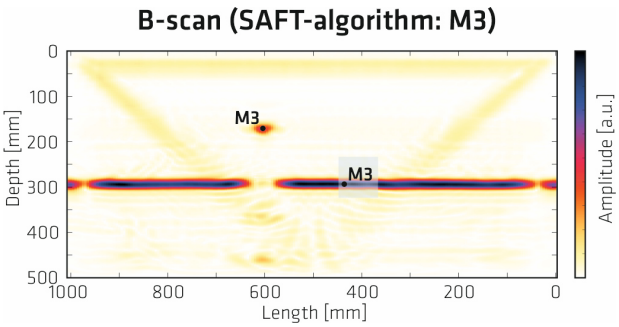

Fig. 7. B-scan of the reconstructed ultrasonic data referring to the reference point M3 (variation S2 without distance error) for the test specimen "Pk218".

Table 2 shows the mean error between the geometrical reconstruction results using the input parameters acc. to Table 1 and the actual dimensions of the test specimen. It can be seen clearly that the mean error for the component thickness is overall not greater than one percent using this approach. At the same time, the mean deviation for the position of the drill hole is larger. This can be explained by the fact that the back wall of the component is the basis for determining the characteristic values (input values).

Table 2. Selected results of the geometrical reconstruction using the input values acc. to Table 1

	Reference point	Mean error - Thickness [mm / %]	Mean error - bore hole [mm / %]
Variation S2	M1	-1.0 / 0.2	0.5 / 0.2
	M2	-0.4 / 0.1	1.4 / 0.6
	M3	-0.4 / 0.1	2.8 / 1.1
	$\bar{M}$	0.6 / 0.1	1.6 / 0.6

Fig. 8 summarizes the results of the reconstruction for the different variations of the determination of the sound velocity ($\bar{c}$) and the lead time (t_0). For reasons of clarity, the results for the different reference points considered in one variation are stated as an average value (cf. Table 2: $\bar{M}$). This results in a mean geometrical error for the variation S2 (S2 - backwall echo + 1st multiple echo) of 0.1 % for the reconstructed backwall and 0.6 % for the borehole without considering the spacing between the probe's transmitter and receiver (a_{TR}).

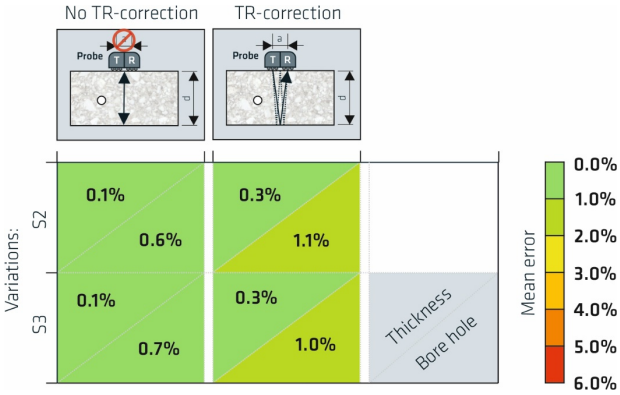

Fig. 8. Result matrix for the mean deviation of the geometrically reconstructed measurement data for the test specimen "Pk218" for the different variations.

In summary, it can be stated for the reference specimen "Pk218" made of polyamide that all presented variants for the determination of the parameters solely based on the measuring data lead to precise results with a maximum mean error in the order of one percent. In this context, it may be interesting to note that a simplified geometrical consideration of the distance between the transmitter and receiver does not improve the results. Quite the contrary, it was observed that the results are slightly less accurate. It is assumed that the simplified geometric consideration is not sufficient for a correction. In particular, effects of diffraction and reflection of the wave field at the upper edge of the borehole must be considered. For this reason, this simplified correction is not used in the following investigations.

4 Concrete specimen

As described in the introduction, the location of tendons as safety-relevant components of a structure is a common testing task. For evaluation and validation purposes, a test specimen with the internal designation "Pk266" was produced at BAM [22], in which different scenarios, such as varying component thicknesses and depth positions of the tendons, are represented. The specimen consists of a concrete with an aggregate with a maximum diameter of $D_{Gk} = 16\ mm$. The geometrical dimensions are shown in Fig. 9. The mounted tendon ducts are filled with air.

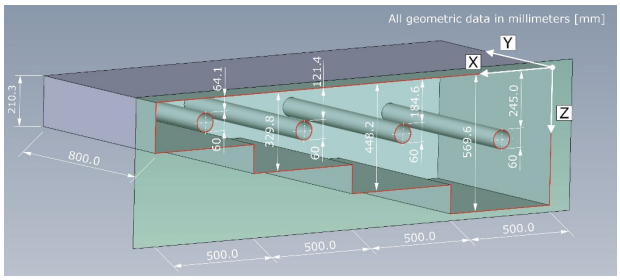

Fig. 9. 3D technical drawing of BAM specimen "Pk266" made of concrete with tendon ducts.

The concrete specimen was scanned with the same system used for the reference specimen "Pk218" with the probe shown in Fig. 2. The grid of measuring points with a spacing of $a = 10\ mm$ starts at a length of $X = 70\ mm$ and ends at $X = 1870\ mm$. The sound velocity $(\bar{c})$ and the time zero (t_0) were determined for different variants using the proposed procedure, and the reconstruction calculation was performed using the InterSAFT software. Fig. 10 shows an example of the geometric reconstruction results in a B-scan for the reference point M3 calibrated on the step with a thickness of $d = 210.3\ mm$. The four echoes reflected at the tendon ducts and the back wall of the different steps can be seen very well. Additionally, for the step with a thickness of $d = 210.3\ mm$ and a thickness of $d = 329.8\ mm$, the first multiple echoes can be seen. Each reconstructed data set consists of 71 B-scans from which the geometrical information for the evaluation is obtained.

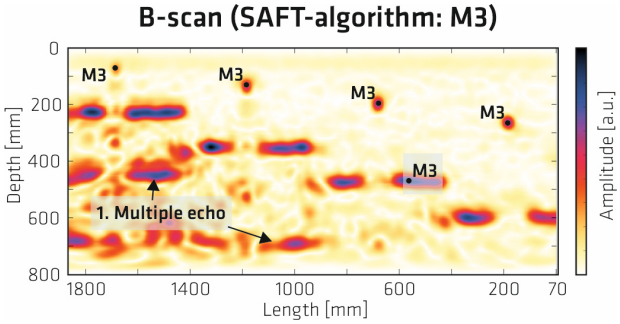

Fig. 10. B-scan of the reconstructed ultrasonic data referring to the reference point M3 (variation S2 without distance error) for the test specimen "Pk266".

A total of 21 data sets (21 variants) were evaluated. Since the correction of the transmitter and receiver spacing when investigating the reference specimen "Pk218" did not result in any significant improvement, the respective results are not shown here. Furthermore, the geometrical results of the evaluation at the reference points (M1, M2, M3) of the signal are summarized to an average value for reasons of clarity and comprehensibility again (compare Table 2). The matrix in Fig. 11 summarizes the results of the geometrical reconstruction calculations.

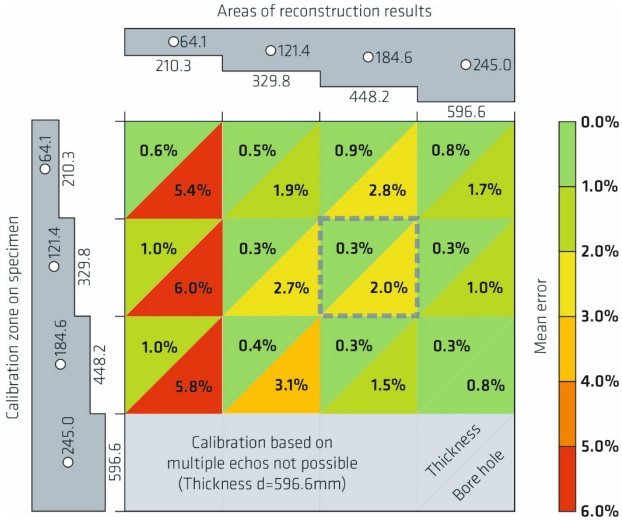

Fig. 11. Result matrix for the mean error of the geometrically reconstructed measurement data from the actual dimensions of the test specimen "Pk266" for the different investigated variations.

The matrix in Fig. 11 is structured as follows: On the left, the schematic representation of the test specimen can be seen in vertical alignment. Each step of the test specimen corresponds to a zone in which the velocity $(\bar{c})$ and time zero (t_0) were determined. In the upper part of the figure, the schematic representation of the test specimen can also be seen – now in horizontal alignment. This represents the geometric assignment of the results on the test specimen. Starting from the zone of calibration, the value of the mean geometric deviation of the component thickness and of the tendon duct position can now be extracted for the respective area. In addition, the deviation is color-coded. For example, the mean geometrical deviation for the reconstructed ultrasonic data calibrated in the area with a thickness of $d = 329.8\ mm$ is about 0.3 % for the component thickness and about 2.0 % for the tendon duct position in the area with a thickness of $d = 448.2\ mm$ (cf. Fig. 11; dashed gray box). At the component thickness of $d = 569.6\ mm$, no calibration and thus no reconstruction could be performed since no multiple echoes could be observed. The respective part of the matrix is therefore shaded in gray.

By color-coding the mean geometrical errors of the reconstructed results, the following simplified summary statements can be made. With the proposed approach, the component thicknesses can be reconstructed with a small mean error of no more than 1 %. As expected, the highest precision in geometrical reconstruction is achieved when the range of calibration and reconstruction are identical

(Mean error max. 0.6 %). As a tendency, the more the range of the calibration and the range of the reconstruction differ geometrically, the more the result of the reconstruction deviates from the actual value. For the results of the geometrical reconstruction of the tension channels, this tendency can be seen even more clearly. For example, the average error for the geometrical position of the tendon duct in a depth of $t = 121.4\ mm$ based on the calibration in the area with a thickness of $d = 448.2\ mm$ is about 3.1 %. In addition, this trend is superimposed by another effect: The greater the mounting depth of the tendon duct, the smaller the geometric error. While the results for the tensioning channels with a depth of $t = 245.0\ mm$ show only a maximum error of 1.7 %, the results for a depth of $t = 64.1\ mm$ show errors of more than 5 %. It must be considered in this context that the choice of reference point plays a significant role in the evaluation of this deviation. While the reference point M1 shows an error of 2.4 % on average for all measurements regarding the duct close to the surface ($t = 64.1\ mm$), this increases to 5.8 % for the reference point M2 and finally to 8.7 % for the reference point M3. This effect also tends to be observed for the other tensioning ducts.

How can these errors for the reconstruction of the tendon duct position be justified? On the one hand, it is observed that if there is a large deviation between the calibration zone and the actual position of the object to be detected, the error increases overall. Possible causes for this are the change of the signal shape with increasing transit time (Fig. 4, (b)) and resulting errors in the calculation of sound velocity $(\overline{c})$ and time zero (t_0). Furthermore, the simplified assumption of neglecting the distance between transmitter and receiver of the probe will play a role. In the previous case study on the reference test specimen, the simplified geometrical assumption did not result in any significant improvements. Nevertheless, the distance seems to have an effect in case of the concrete specimen, so that further investigations are required in this respect. On the other hand, it is observed that the choice of the reference point in the ultrasonic signal becomes important, especially for the tendon ducts that are close to the surface. It is basically known in ultrasonic measurements that there is a zone in which objects can only be detected to a limited extent due to the surface waves. This depth range is referred to as the "dead zone" [23], depends on the frequencies, and covers in concrete testing a few centimeters. The tendon duct with a depth of $t = 64.1\ mm$ is already close to this range, so that it can be assumed here that there are superpositions with the surface waves which have an unfavorable effect on the results of the geometrical reconstruction. Another influence results from the idealized underlying boundary conditions of the SAFT algorithm: The algorithm assumes an idealized point-shaped reflector. In reality, the tendon ducts have larger diameters of, e. g. in this specific case, ca. $D = 63\ mm$, which corresponds to a locally strongly curved reflector. This deviation can additionally lead to an error in the reconstruction, which should be considered separately.

6 Conclusion

This article describes a procedure for determining input parameters (sound velocity and time zero) required for the reconstruction of structural components in ultrasonic testing and the effects on the result of the geometrical reconstruction. Due to the large range of variation for the different concrete mixtures, the advantage is that the parameters can be obtained directly from the measured data without having to perform additional measurements (calibration measurements) on the structure or on extracted specimens (drill core). The basic procedure is demonstrated on two test specimens using the same measurement technique: First, on a reference test block made of polyamide to exclude interfering influences from scattering at the aggregate in the concrete; second, on a concrete specimen with different geometrical boundary conditions (component thickness and mounting depth of the tendon ducts).

As a result of the investigations, a comparative presentation of different variants shows that the described procedure is suitable to perform a sufficiently accurate geometric reconstruction for the position of tendons and component thicknesses solely from the measured data. The achieved accuracies depend on the different boundary conditions and assumptions. The relative error for deeper tendon ducts is smaller (min. err. 0.8 %) than for tendons closer to the measurement surface (max. err. 6.0 %). This result is significantly influenced by the choice of the reference points in the signal, the consideration of the geometry of the aperture of the measurement technique as well as the differences between the position of the objects of interest and the depth range in which the sound velocity and time zero were calibrated.

References

1. IAEA-International Atomic Energy Agency, Guidebook on non-destructiv testing of concrete structures, TRAINING COURSE SERIES No. 17, 17th edn, VIENNA, (2002).
2. Bergmeister, K. and Rostan, S., Monitoring and safety evaluation of existing concrete structures: bulletin 22. state-of-the-art report. Bulletin **22** (2003).
3. DMJM HARRIS, TEST AND ASSESSMENT OF NDT METHODS FOR POST-TENSIONING SYSTEMS IN SEGMENTAL BALANCED CANTILEVER CONCRETE BRIDGES (2003).
4. Gucunski, N., Imani, A., Romero, F., Nazarian, S., Yuan, D., Wiggenhauser, H., Shokouhi, P., Taffe, A., Kutrubes, D., Nondestructive Testing to Identify Concrete Bridge Deck Deterioration, REPORT S2-R06A-RR-1, Transportation Research Board, Washington, D.C. (2012).
5. Beushausen, H. and Fernandez Luco, L. (eds), Performance-Based Specifications and Control of Concrete Durability: State-of-the-Art Report RILEM TC 230-PSC, 1st edn, Springer, Dordrecht (2015).

6. Feistkorn, S., Taffe, A., Methods to Assess the Quality of Non-Destructive Testing in Civil Engineering Using POD and GUM for Static Calculations of Existing Structures. Materials Testing, Band **56** (7-8), 611–616 (2014).
7. Feistkorn, S., Rebar detection — POD approach to determine the reliability of GPR systems and to quantify the influence of different material parameters, in The proceedings of 2016 16th International Conference on Ground Penetrating Radar (GPR): 13-16 June 2016, The Hong Kong Polytechnic University, Department of Land Surveying and Geo-Informatics. 2016 16th International Conference on Ground Penetrating Radar (GPR), Hong Kong, Hong Kong. IEEE, Piscataway, NJ, pp. 1–6 (2016).
8. Feistkorn, S., Algernon, D., Scherrer, M., POD and GUM Universal Methods for Making Safety Measurable. Journal of Safety Studies, **2** (2), 56 (2016).
9. Keßler, S., Probabilistic corrosion condition assessment of a tunnel structure. Structural Concrete, **21** (4), 1345–1355 (2020).
10. JCGM - Joint Committee for Guides in Metrology, Evaluation of measurement data — Guide to the expression of uncertainty in measurement (2008).
11. JCGM - Joint Committee for Guides in Metrology, Evaluation of measurement data - Supplement 1 to the GUM — Propagation of distributions using a Monte Carlo method (2008).
12. Braml, T., Taffe, A., Feistkorn, S., Wurzer, O., Assessment of Existing Structures using Probabilistic Analysis Methods in Combination with Nondestructive Testing Methods. Structural Engineering International, **23** (4), 376–385 (2013).
13. Küttenbaum, S., Maack, S., Taffe, A., Structural safety referring to ultrasound on concrete bridges. Beton- und Stahlbetonbau, **113** (4), 7–13 (2018).
14. Küttenbaum, S., Feistkorn, S., Braml, T., Taffe, A., Maack, S., Methods to Quantify the Utility of NDT in Bridge Reassessment. Lecture Notes in Civil Engineering, Springer International Publishing (2021).
15. Küttenbaum, S., Braml, T., Taffe, A., Keßler, S., Maack, S., Reliability assessment of existing structures using results of nondestructive testing. Structural Concrete, **23**, 403 (2021).
16. Küttenbaum, S., Braml, T., Taffe, A., Maack, S., Towards NDT-supported decisions on the reliability of existing bridges, in ICOSSAR 2021-2022: 13th Internation Conference on Structural Safety & Reliabilty. ICOSSAR 2021-2022, 13-17 September 2022, Tongji University, Shanghai, China, pp. 1–10 (2022). (accepted)
17. Matthews, S., Bigaj-van Vliet, A., Walraven, J., Mancini, G., Dieteren, G., fib Model Code 2020: Towards a general code for both new and existing concrete structures. Structural Concrete, **19** (4), 969–979 (2018).
18. Matthews, S., Mancini, G., Alexander, M.G., Beushausen, H., Dehn, F., Moyo, P., Forensic engineering - fib MC 2020 and existing structures. MATEC Web Conf., **199**, 1–14 (2018).
19. S. Maack, S. Küttenbaum, N., Epple, M. Aligholizadeh, Die Ultraschall-Echomethode – von der Messung zur bautechnischen Kenngröße: Studie zur Leistungsfähigkeit der Messmethode am Referenzmaterial Polyamid und an Beton. Beton- und Stahlbetonbau, **22** (6), 270 (2021). (German)
20. S. Maack, S. Küttenbaum, B. Bühling, E. Niederleithinger, Low frequency ultrasonic dataset for pulse echo object detection in an isotropic homogeneous medium as reference for heterogeneous materials in civil engineering, Data in Brief, 42, 108235 (2022).
21. Krause, M., Mayer, K., Friese, M., Milmann, B., Mielentz, F., Ballier, G., Progress in ultrasonic tendon duct imaging. European Journal of Environmental and Civil Engineering, **15** (4), 461–485 (2011).
22. Reinhardt, H.W., Zerstörungsfreie Strukturbestimmung von Betonbauteilen mit akustischen und elektromagnetischen Echo-Verfahren: Abschlussbericht Forschergruppe FOR384, Anhang - Liste der erstellten Prüfkörper (2007). (German)
23. DIN 2010, DIN EN 1330-04:2010-05, Materialprüfnormen für metallische Werkstoffe (engl.: Non-destructive testing – Terminology Part 4: Terms used in ultrasonic testing; Trilingual version), Deutsches Institut für Normung e.V., Berlin (2010).